

## Analysis of key mechanical parameters and their relations with brittleness in triaxial failure test

Jiali Ren\*, De-hua Han and Yang Wang, RPL, University of Houston; Yonghao Zhang, China Petroleum Logging Company; Luanxiao Zhao, Tongji University.

### Summary

Triaxial failure test as a traditional experiment is used to study rock mechanical behavior. We have tested 5 reservoir rock samples to investigate several key mechanical parameters including the crack initiation stress ( $C_i$ ), the crack damage stress ( $C_d$ ) and the ratios of  $C_i$  and  $C_d$  to compressive strength ( $C_i/CP$  and  $C_d/CP$ ). They are analyzed by comparing with elastic moduli and rock brittleness. Based on the measured data, we have built several correlations to describe how the key mechanical parameters relate to elastic moduli and brittleness. The results indicate  $C_i$  and  $C_d$  show positive with elastic moduli and the ratio of crack damage stress and compressive strength ( $C_d/CP$ ) is a good indicator to evaluate rock brittleness.

### Introduction

In order to obtain a better understanding on rock mechanics for hydraulic fracturing in unconventional reservoirs, laboratory investigations are tested, especially for triaxial failure test. Traditionally, compressive strength ( $C_p$ ), elastic moduli and brittleness are used to integrate rock rupture. In this work, we introduce the crack initiation stress ( $C_i$ ) and the crack damage stress ( $C_d$ ) as new key parameters to describe failure behaviors. The crack initiation stress and the crack damage stress for igneous rocks are investigated extensively, but for reservoir rocks, there are not too much research about  $C_i$  and  $C_d$ . In progressive brittle fracture processes,  $C_i$  and  $C_d$  are distinguishing stress points can determine cracks development and deformation identification in different stages.

Based on strain-stress behavior of a loaded material (Figure.1), Brace (1964) and Bieniawski (1967) defined these stages as being (1) crack closure, (2) linear elastic deformation, (3) crack initiation and stable crack growth, (4) critical energy release and unstable crack growth, and (5) failure and postpeak stage. Crack closure occurs in the initial loading stage when preexisting cracks orientated at an angle to applied load close. Once the majority of preexisting cracks closed, linear elastic deformation takes place and static Young's modulus and Poisson's ratio are derived from strain-stress curve. The crack initiation stress represents the stress level where micro-cracks start to generate and is the onset of nonlinear part. Martin (1993) and Eberhardt et al. (1998) discussed stable tensile cracks start to increase from the crack initiation stress and crack growth can be stopped by controlling the applies load. Unstable crack growth occurs at the point of reversal in volumetric strain curve and

this stress point is the crack damage stress where shear cracks start to increase dramatically.

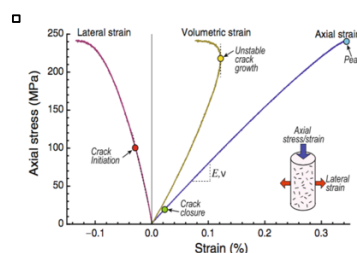


Figure 1. Strain-stress response in compressive test (modified after Nicksiar and Martin, 2013).

In our study, we focus on  $C_i$ ,  $C_d$ ,  $C_i/CP$  and  $C_d/CP$  from pre-peak stage as important mechanical parameters. We try to analyze their performance on rock failure evaluation by correlating them with three brittleness indices and elastic moduli.

### Sample description and Experimental procedures

Five reservoir rock samples including three shales and two sandstones are measured in triaxial failure experiment. For sandstones, porosity and density of Brea sandstone (BR) are 23.33% and 2.62 g/cm<sup>3</sup>, porosity and density of Idaho Gray sandstone (IG) are 33.3% and 2.57 g/cm<sup>3</sup>. For shale, we test two Mancos shales including vertical and horizontal coring (MV and MH), and a Xinjiang shale (XJ). Porosities are from 4.83% to 6.72% and densities are from 2.41 g/cm<sup>3</sup> to 2.52 g/cm<sup>3</sup>. The thin section images are taken under cross-polarized light for each sample. Two sandstones are mainly composed of angular quartz, however, different with point contacts in Brea sandstone, Idaho Gray sandstone shows more surface contacts. For shales, they all have very fine grains. Two Mancos shales both have belt quartz concentration and lots of organic matters are filled with in pore spaces in Xinjiang shale. Figure 2 shows two typical thin section images for Brea sandstone and Mancos shale (vertical).

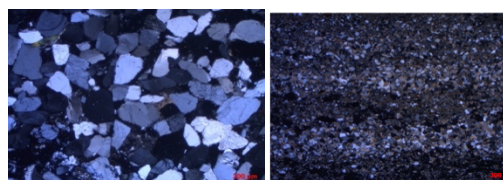


Figure 2: Thin section images for (left) Brea sandstone and (right) Mancos shale (vertical)

## Rock mechanical parameters in triaxial failure test

Experiments are performed with the NER Auto 1500 triaxial apparatus in China Petroleum Logging Company. The diameter for each cylindrical sample is 1.5 inch and specimens undergo failure tests in triaxial stress condition without pore pressure. In vertical direction, the strain is measured with linear variable differential transformers (LVDT), while radial strain is obtained by one pair of strain gauges on side. A typical procedure starts from hydrostatic confining pressure which is fixed at 20 Mpa, then axial loading is introduced with fixed strain rate which is suggested by ISRM until it experiences whole failure process.

### Methodology

#### 1. Methods for $C_i$ , $C_d$ and $C_p$

For the crack initiation stress, Brace et al. (1996) noted that the onset of dilatancy could be established using volumetric strain by examining when the volumetric strain deviated from early linear part. Then Martin and Chandler (1994) discussed that crack initiation is difficult to identify from volumetric strain-stress curve if the sample contains many preexisting cracks. They proposed crack volumetric strain-stress curve can determine  $C_i$  and crack volumetric strain is obtained by subtracting the elastic volumetric strain from the total volumetric strain. More recently, Nicksiar and Martin (2012) introduced a new method that relies on the lateral strain response (LSR). The LSR from zero stress to crack damage stress is examined for changed as axial stress applied. In order to detect changes in the LSR, the loading response is compared with a linear reference line taken from zero point to the crack damage stress.  $C_i$  is determined by fitting a best-fitted parabola and selecting the stress associated with maximum strain difference (Figure 3).  $C_i$  from the LSR method has a perfect fitting with  $C_i$  based on crack volumetric strain method. In this work, we use the LSR method to identify  $C_i$ .

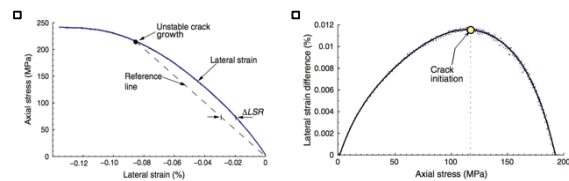


Figure 3. The methodology used to establish  $C_i$  using the lateral strain response. (Left) Illustration of the LSR methodology. (Right) Example of the LSR result (Nicksiar and Martin, 2012).

Based on strain-stress curves measured from the failure test,  $C_d$  can be determined easily by finding the reversal point of volumetric strain. Meanwhile, the peak stress, as rock compressive strength ( $C_p$ ), is also derived from peak point on strain-stress curve.

#### 2. Methods for elastic moduli and brittleness indices.

In order to investigate the roles of  $C_i$  and  $C_d$  in rock failure evaluation, we selected Young's modulus, Poisson's ratio and brittleness as traditional important mechanical parameters to compare with  $C_i$  and  $C_d$ . Young's modulus and Poisson's ratio we use in this study are static moduli, which are detected from the linear elastic part of strain-stress curve. Young's modulus could be derived from slope of axial strain and axial stress curve and Poisson's ratio is acquired from axial strain and lateral strain.

Brittleness as a crucial parameter to judge if a rock can be ruptured easily, can be evaluated quantitatively based on different definitions. We choose three brittleness indices based on strain change, mineralogy and energy conversation. For strain change method, rock is considered as brittle if it experiences more elastic deformation stage. Hukka and Das suggested using the ratio of elastic strain ( $\epsilon_{el}$ ) to total strain ( $\epsilon_{tot}$ ) in pre-peak stage as brittleness index. B1 is derived from Equation 1.

$$B1 = \frac{\epsilon_{el}}{\epsilon_{tot}} \quad (1)$$

where,  $\epsilon_{tot} = \epsilon_{el} + \epsilon_{pl}$ ,  $\epsilon_{pl}$  is the plastic strain in pre-peak stage.

The second method to gain brittleness depends on rock mineralogy. Jarvie et al. argued that the contents of quartz can significantly affect rock brittleness. They defined brittleness index as the weight fraction of quartz to estimate rock brittleness. B2 is showed in Equation 2.

$$B2 = \frac{W_{quartz}}{W_{tot}} \quad (2)$$

Additionally, we proposed a new brittleness index based on energy conversion. In Figure 4, Ai et al. discussed models of energy conversion from strain-stress curves for brittle and ductile materials and different colors in strain-stress curves represent various energy parts. In pre-peak stage, the strain-stress curve of ductile material (Figure 4a) indicates more plastic energy (green part), yet it shows more elastic energy accumulated (red part) and a steeper yield platform for brittle material (Figure 4b). In post-peak stage, the blue part and gray part represent respectively the rock fracture energy and the unconsumed energy. For ductile material, the elastic energy stored in pre-peak stage is not enough to complete the failure process without extra input energy (part with yellow dash line). For brittle material, it has sufficient stored energy to rupture and still has excess energy (yellow part) released. So we propose a new brittleness index based on the analysis of energy conversion in Equation 3.

$$B3 = \left(0.5 - \frac{W_d}{2W_p}\right) + \left(0.5 - \frac{W_u}{W_e}\right) \quad (3)$$

## Rock mechanical parameters in triaxial failure test

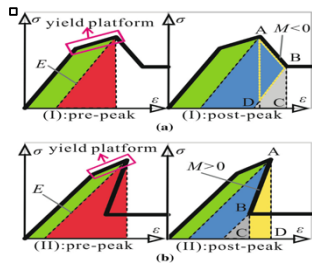


Figure 4. Schematic diagrams of energy conversion during rock failure (modified after Ai et al. 2016).

In which,  $W_d$  is plastic energy (red part),  $W_u$  represents unconsumed energy (gray part),  $W_p$  is total energy in pre-peak stage including elastic energy and plastic energy.  $W_e$  is the stored elastic energy (red part). For brittle rock, we consider it has more stored elastic energy in pre-peak stage and less unconsumed energy from stored energy in post-peak stage.

### Data Analysis and discussions

Triaxial failure tests provide us strain-stress curves of different rock specimens, then we obtain  $C_i$ ,  $C_d$ ,  $C_p$ , static moduli and three brittleness indices. First of all,  $C_i/C_p$  and  $C_d/C_p$  for different rocks are studied. From previous research, the crack initiation stress is located at a stress level of about 30-50% of the peak strength and the crack damage stress is about 70-80% of the peak strength when confined. There are lots of data about  $C_i/C_p$  and  $C_d/C_p$  for igneous rocks, but few for reservoir rocks. Figure 5 shows relations of porosity with  $C_i/C_p$  and  $C_d/C_p$ . The ratios of  $C_i$  to  $C_p$  are from 0.37 to 0.42 and the ratios of  $C_d$  to  $C_p$  are in a range from 0.67 to 0.75. Although the ranges for these two ratios are narrow, the ratios show difference for each rock. In the plots, the blue circle point represents shale and the yellow triangle point indicates sandstone.

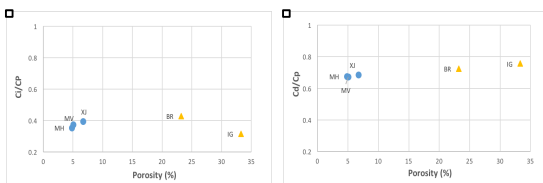


Figure 5. Plots of porosity with  $C_i/C_p$  and  $C_d/C_p$

In Figure 6,  $C_i$  and  $C_d$  are correlated with static Young's modulus and Poisson's ratio from strain-stress curves. As Figure 6 showing,  $C_i$  and  $C_d$  have a positive relation with Young's modulus and the correlation with  $C_i$  is better than the correlation with  $C_d$ . The  $R^2$  can reach to 0.96 and 0.92. Figure 7 are clearly shown that Poisson's ratio also has same relation with  $C_i$  and  $C_d$  as Young's modulus. However, the

fitting results are not perfect and  $R^2$  is about 0.56. This positive relation can be observed obviously on sandstones, but for shales, the points are slightly scattering.

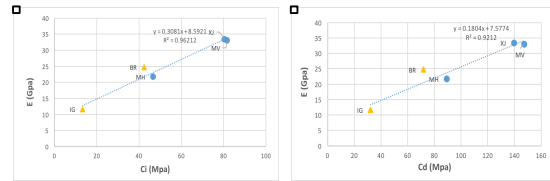


Figure 6. Plots of Young's modulus with  $C_i$  and  $C_d$

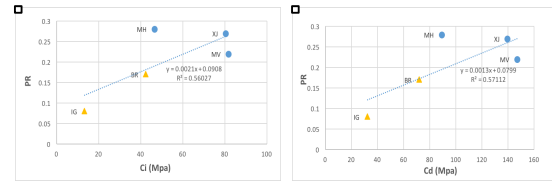


Figure 7. Plots of Poisson's ratio with  $C_i$  and  $C_d$

Moreover,  $C_i/C_p$  and  $C_d/C_p$  are also compared with elastic moduli in Figure 8 and Figure 9. In Figure 8, Young's modulus is compared with  $C_i/C_p$  and  $C_d/C_p$ . We find the different relations for them: the correlation between  $C_i/C_p$  and Young's modulus is positive, yet  $C_d/C_p$  decreases with Young's modulus increasing. The relations of Poisson's ratio with  $C_i/C_p$  and  $C_d/C_p$  are plotted in Figure 9. Similarly,  $C_i/C_p$  shows positive relation with Poisson's ratio.  $C_d/C_p$  has an opposite relation with Poisson's ratio. When comparing with elastic moduli,  $C_i$  and  $C_d$  has same relations with them and both increase with elastic moduli increasing. However,  $C_i/C_p$  and  $C_d/C_p$  shows different relations with elastic moduli. We consider  $C_i/C_p$  is close to elastic stage and has a strongly positive relation with elastic moduli. However,  $C_d/C_p$  which indicates the weight of unstable part in plastic stage can have an opposite relation with elastic moduli.

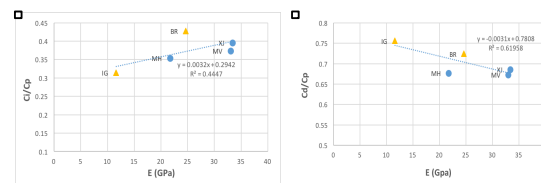


Figure 8. Plots of Young's modulus with  $C_i/C_p$  and  $C_d/C_p$

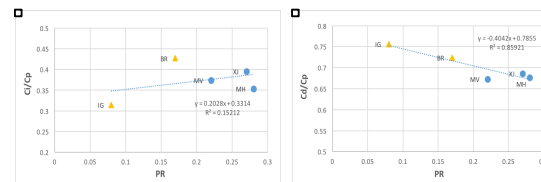


Figure 9. Plots of Poisson's ratio with  $C_i/C_p$  and  $C_d/C_p$

## Rock mechanical parameters in triaxial failure test

Brittleness indices as an important parameter to describe rock failure behavior are introduced to analyze  $C_i$ ,  $C_d$ ,  $C_i/C_p$  and  $C_d/C_p$ . On the basis of different methods, three brittleness indices, B1, B2 and B3 are consistent on brittleness evaluation. Firstly, we tested the correlations of  $C_i$  and  $C_d$  with brittleness indices and the results show that  $C_i$  and  $C_d$  cannot correlated with brittleness indices. For sandstone, high brittleness indices show low  $C_i$  and  $C_d$ , but for shale, the relations change to negative. So depending on the experimental data, we believe  $C_i$  and  $C_d$  cannot be used as indicator to evaluate rock brittleness and will not show the results in the figure.

If  $C_i/C_p$  and  $C_d/C_p$  are compared with brittleness indices, the results are different. Figure 10 is plotted by  $C_i/C_d$  and brittleness indices. In the correlations with B1, B2 and B3,  $C_i/C_p$  shows roughly negative relation. Even though the correlations of  $C_i/C_p$  and brittleness indices are not good for sandstones, the negative relation can be observed on shale. If  $C_i/C_p$  is low, the rock starts to create tensile cracks in relatively early stage and is considered as brittle.  $C_i/C_p$  describes the ability to generate stable cracks which is in a controllable situation. It is different with the unstable situation in failure condition, so  $C_i/C_p$  cannot represent the whole rupture and doesn't correlate with brittleness indices well.

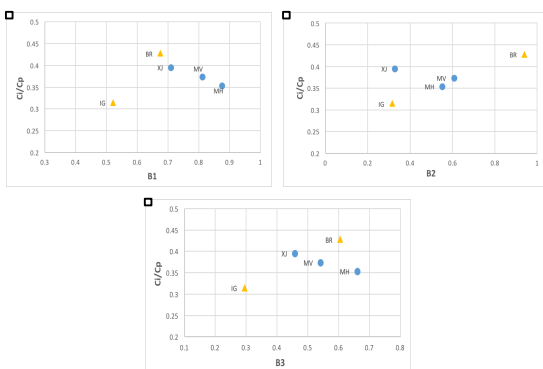


Figure 10. Plots of  $C_i/C_p$  with brittleness indices

In Figure 11,  $C_d/C_p$  and brittleness indices are plotted.  $C_d/C_p$  is found to correlated with brittleness indices well for all samples. The relation between them is negative and high brittleness index suggests low  $C_d/C_p$ . In the comparison between  $C_d/C_p$  and B2, the perfect trend line cannot be gained from all data points, but the strong correlation is shown on each kind of rock samples. Based on the relations of  $C_d/C_p$  with brittleness indices, Although  $C_d/C_p$  is in a narrow span, it can be considered as a new parameter to

evaluate failure behavior and estimate brittleness. High  $C_d/C_p$  means the rock enter unstable stage in relatively high stress condition and it need more energy to complete rupture process, so the rock is ductile with low brittleness index.

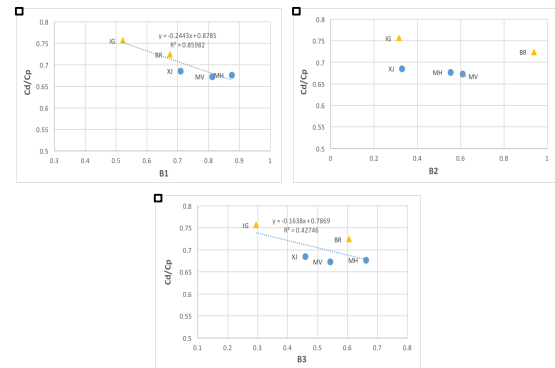


Figure 11. Plots of  $C_d/C_p$  with brittleness indices

## Conclusion

Triaxial failure experiments on reservoir rock specimens are tested to analyze  $C_i$ ,  $C_d$ ,  $C_i/C_p$ ,  $C_d/C_p$  and their relations with elastic moduli and brittleness in this work. After comparing with elastic moduli,  $C_i$  and  $C_d$  correlate positively well with Young's modulus and Poisson's ratio. However,  $C_i/C_p$  and  $C_d/C_p$  shows different relations with elastic modulus. When  $C_i/C_p$  rises, elastic moduli increase. For  $C_d/C_p$ , a larger ratio of  $C_i$  to  $C_p$  suggests smaller elastic moduli. When comparing with brittleness indices,  $C_i$  and  $C_d$  don't show good fitting and we cannot only use  $C_i$  or  $C_d$  to predict brittleness. If we use  $C_i/C_p$  and  $C_d/C_p$  to compare with brittleness indices, better correlations are observed. For shales,  $C_i/C_p$  shows consistent results on brittleness evaluation, but the results for sandstones are not acceptable. The correlations of  $C_d/C_p$  and brittleness indices are perfect and  $C_d/C_p$  has an excellent performance on brittleness prediction. We conclude  $C_i$  and  $C_d$  as key parameters show mechanical properties in different stages and are related to elastic moduli.  $C_i/C_p$  and  $C_d/C_p$  are better than  $C_i$  and  $C_d$  to describe how the rock deform and cracks develop in different stages.  $C_d/C_p$  as a key parameter from pre-peak stage shows great results on failure description and brittleness evaluation when correlating with brittleness indices.

## Acknowledgements

The work is supported by Fluids/DHI consortium. The experimental measurements are provided by China Petroleum Logging Company. The authors would like to express the gratitude them.

## REFERENCES

- Ai, C., J. Zhang, Y. Li, J. Zeng, X. Yang, and J. Wang, 2016, Estimation criteria for rock brittleness based on energy analysis during rupturing process: *Rock Mechanics and Rock Engineering*, **49**: 4681–4698, <https://doi.org/10.1007/s00603-016-1078-x>.
- Bieniawski, Z. T., 1967a, Mechanism of brittle fracture of rock, Part I—Theory of the fracture process: *International Journal of Rock Mechanics and Mining Sciences & Geomechanics Abstracts*, **4**, 395–406, [https://doi.org/10.1016/0148-9062\(67\)90030-7](https://doi.org/10.1016/0148-9062(67)90030-7).
- Bieniawski, Z. T., 1967b, Mechanism of brittle fracture of rock, Part II—Experimental studies: *International Journal of Rock Mechanics and Mining Sciences & Geomechanics Abstracts*, **4**, 407–423, [https://doi.org/10.1016/0148-9062\(67\)90031-9](https://doi.org/10.1016/0148-9062(67)90031-9).
- Brace, W. F., B. Paulding, and C. Scholz, 1966, Dilatancy in the fracture of crystalline rocks: *Journal of Geophysical Research*, **71**, 3939–3953, <https://doi.org/10.1029/JZ071i016p03939>.
- Hucka, V., and B. Das, 1974, Brittleness determination of rocks by different methods: *International Journal of Rock Mechanics and Mining Sciences & Geomechanics Abstracts*, **11**, 389–392, [https://doi.org/10.1016/0148-9062\(74\)91109-7](https://doi.org/10.1016/0148-9062(74)91109-7).
- Jarvie, D. M., R. J. Hill, T. E. Ruble, and R. M. Pollastro, 2007, Unconventional shale-gas systems: The Mississippian Barnett Shale of north-central Texas as one model for thermogenic shale-gas assessment: *AAPG Bulletin*, **91**, 475–499, <https://doi.org/10.1306/12190606068>.
- Martin, C. D., and N. A. Chandler, 1994, The progressive fracture of Lac du Bonnet granite: *International Journal of Rock Mechanics and Mining Sciences & Geomechanics Abstracts*, **31**, 643–659, [https://doi.org/10.1016/0148-9062\(94\)90005-1](https://doi.org/10.1016/0148-9062(94)90005-1).
- Nicksiar, M., and C. D. Martin, 2012, Evaluation of Methods for determining crack initiation in compression tests on low-porosity rocks: *Rock Mechanics and Rock Engineering*, **45**, 607–617, <https://doi.org/10.1007/s00603-012-0221-6>.